Food Microbiology 88 (2020) 103399

Contents lists available at ScienceDirect

Food Microbiology

journal homepage: www.elsevier.com/locate/fm

Metabolic characterisation of eight *Escherichia coli* strains including "Big Six" and acidic responses of selected strains revealed by NMR spectroscopy

Lin Chen[a,c], Xue Zhao[a,c], Ji'en Wu[b], Qin Liu[a,c], Xinyi Pang[a,c], Hongshun Yang[a,c,*]

[a] Department of Food Science and Technology, National University of Singapore, Singapore, 117542, Singapore
[b] Setsco Services Pte., Ltd., Singapore, 608925, Singapore
[c] National University of Singapore (Suzhou) Research Institute, 377 Lin Quan Street, Suzhou Industrial Park, Suzhou, Jiangsu, 215123, PR China

ARTICLE INFO

Keywords:
Metabolomics
Principal component analysis
Acid stress
Pathway analysis
NMR
Escherichia coli O157:H7

ABSTRACT

The metabolic diversity of *Escherichia coli* strains (non-pathogenic *E. coli* ATCC 25922, and pathogenic *E. coli* O157:H7, O26:H11, O45:H2, O103:H11, O111, O121:H19, and O145) was tested using nuclear magnetic resonance. Based on two representative two-dimensional ^{1}H–^{13}C spectra, 38 metabolites were identified in *E. coli* intracellular samples. Principal component analysis indicated that metabolites including lysine, arginine, α-ketoglutaric acid, adenosine, and fumaric acid were responsible for the separation of *E. coli* ATCC 25922. Relatively large metabolic differences between ATCC 25922 and the pathogenic strains were recoded. The most varied pairwise group (ATCC 25922 *vs.* O26:H11) was further analysed. The screened metabolites and enrichment pathway tests revealed different amino acid metabolism and higher requirement for energy production in the pathogenic strains. The acidic responses of the selected strains were further tested. The *in vitro* and *in vivo* inactivation kinetics, morphological changes, and protein leakage showed higher acid tolerance of *E. coli* O26:H11. Metabolic analysis of the two strains under acidic stress revealed alternative metabolites and pathways in the two groups. Pathogenic O26:H11 was characterised by higher energy production and amino acid metabolism (lysine and glutamic acid). Real-time PCR tests confirmed that glutamic acid dependent decarboxylase/antiporter system was the major acid resistance mechanism.

1. Introduction

Each year, about 600 million illnesses and 420,000 deaths worldwide occur because of contamination by foodborne pathogens. Infections caused by *Escherichia coli*, *Listeria monocytogenes*, *Salmonella*, and *Campylobacter jejuni* are responsible for the majority cases (Feng et al., 2018; Han et al., 2018). *E. coli* are Gram-negative, rod-shaped, facultatively anaerobic, and non-spore-forming bacteria that comprise various subgroups. Most groups are part of the normal human bacterial gut flora but certain groups are pathogenic and can cause illnesses such as diarrhea and hemolytic uremic syndrome (HUS) (Tomat et al., 2018). These pathogenic *E. coli* are highly adaptive to environmental stresses and food products can be contaminated by *E. coli* at each stage of the human food chain (Liu et al., 2019).

Among the diverse *E. coli* serotypes, *E. coli* O157 is considered as the major life-threatening pathogen. A previous study revealed that annually, *E. coli* O157:H7 causes 63,000 illnesses with a 46.2% hospitalization rate in the USA (Vidovic and Korber, 2016). Its disease progression is characterised by bloody diarrhea and HUS. O157:H7 is grouped with the enterohemorrhagic *E. coli*, a subset of Shiga toxin-producing *E. coli* (STEC). O157:H7 also produces other virulence factors, such as intimin (Gómez-Aldapa et al., 2016). In addition to O157:H7, other serotypes producing Shiga toxins attract attentions recently. Non-O157 STEC infection is estimated to be responsible for 113,000 cases of acute illnesses each year (Diodati et al., 2016). Six non-O157 *E. coli* serogroups (O26, O45, O103, O111, O121, and O145), known as the "big six", were identified as the most common types found in foods by the US Food and Drug Administration (Sheen et al., 2015). Surveillance of the "big six" was limited and only after 2012, the Food Safety and Inspection Service begin to test both O157:H7 and the "big six" in ground beef (Sheen et al., 2015).

Recent studies have clarified different aspects of the "big six", such as rapid detection, inactivation methods, virulence factors, and molecular mechanisms, to help reduce the risk of infection and enhance food safety (Ås et al., 2018; Hsu et al., 2015). For example, Hsu et al. (2015) showed that high pressure processing effectively inactivated the "big six" and *E. coli* O157:H7 in ground beef. In addition, a genomic comparison of two O111 strains revealed differences in single-nucleotide

* Corresponding author. Department of Food Science and Technology, National University of Singapore, Singapore, 117542, Singapore.
E-mail address: fstynghs@nus.edu.sg (H. Yang).

https://doi.org/10.1016/j.fm.2019.103399
Received 10 April 2019; Received in revised form 24 November 2019; Accepted 7 December 2019
Available online 11 December 2019
0740-0020/

polymorphisms (SNPs), which might be responsible for their different virulence (McAllister et al., 2016). However, little information about the global characteristics of the "big six" is available. The emerging nuclear magnetic resonance (NMR) provide a feasible strategy to acquire comprehensive metabolic profiles of microorganisms. For example, the global metabolic responses of *E. coli* and *Listeria* treated with electrolyzed water were studied by our previous reports (Liu et al., 2017b; Liu et al., 2018; Zhao et al., 2019b). By monitoring the changes of microbial metabolomics, a precise snapshot of cells with different physicochemical states can be obtained. Thus, the metabolomics analysis of the "big six" may provide valuable insights into the serotype diversity of STEC.

The aim of the present study was to investigate the overall metabolic differences among eight typical *E. coli* strains from different serotypes. In addition, the acidic responses of selected strains were tested. In the present work, the intracellular metabolites in eight *E. coli* strains were extracted and identified using their NMR spectra. The strains were separated based on the principal metabolites screened by principal component analysis (PCA). The representative strains were selected and the pathway differences between pairwise strains were further analysed by enrichment pathway analysis. In addition, the differential responses of selected *E. coli* strains under acidic stress were assayed using NMR and verified by quantitative real-time PCR (qPCR).

2. Materials and methods

2.1. Bacterial strains and culture condition

Eight *E. coli* strains from different serotypes [non-pathogenic *E. coli* ATCC 25922, and pathogenic *E. coli* O157:H7 (ATCC 43895), O26:H11 (ATCC BAA-2196), O45:H2 (ATCC BAA-2193), O103:H11 (ATCC BAA-2215), O111 (ATCC BAA-2440), O121:H19 (ATCC BAA-2219), and O145 (ATCC BAA-2192)] were used in this study. The strains were inoculated into 10 mL of Tryptone Soya Broth (TSB, Oxoid, Basingstoke, UK) and incubated at 37 °C overnight for resuscitation. The prepared culture was further inoculated into 20 mL of fresh TSB (1:100, v/v) and cultured for 18 h (37 °C). The cultures with around 8 log colony forming units (CFU)/mL were centrifuged at 4500 × *g* (to avoid cell damage at high speed) for at least 10 min (24 °C) and the obtained cell pellets were washed by 0.1 M phosphate-buffered saline (PBS, pH 7.2). After centrifugation, the pellets of the eight *E. coli* strains were used for subsequent metabolites extraction.

2.2. Extraction of E. coli intracellular metabolites

The prepared *E. coli* pellet was immediately mixed with 1 mL of ice-cold methanol-d_4 (Cambridge Isotope Laboratories, Tewksbury, MA, USA) and frozen in liquid nitrogen (Winder et al., 2008). The mixture was then thawed on ice and further frozen in liquid nitrogen. The freeze-thaw cycles were conducted three times to destroy the membrane structure. The mixture was subsequently extracted at −20 °C overnight and the metabolic extract was obtained by centrifugation at 12,000 × *g* for 20 min (4 °C). Trimethylsilylpropanoic acid (TSP, dissolved in methanol-d_4, 10 mM) was mixed with the collected extract as an internal reference (final concentration: 1 mM). The obtained supernatant (600 μL) was immediately subject to NMR test. Three biological replicates of each strain were determined.

2.3. NMR analysis of E. coli metabolic profiles

The prepared samples were determined using a Bruker DRX-500 NMR spectrometer (Bruker, Rheinstetten, Germany). The standard Bruker NOESY pulse sequence (noesypr1d) was applied to obtain the ^{1}H spectrum of each sample and the data were collected using a 10.0 ppm spectral width. Furthermore, the free induction decays were multiplied by an exponential function equivalent to a 1-Hz line-broadening factor before Fourier transformation (Chen et al., 2020). For the subsequent identification of metabolic chemicals, the 2D ^{1}H–^{13}C heteronuclear single quantum coherence spectroscopy (HSQC) of two representative *E. coli* samples (*E. coli* ATCC 25922 and O145) was acquired using the Bruker hsqcedetgpsisp2.3 pulse sequence at 25 °C. The ^{1}H spectra with a width of 10.0 ppm and the ^{13}C spectra with a width of 180.0 ppm were tested in the F2 and F1 channels, respectively (Chen et al., 2019b; Zhao et al., 2019c).

2.4. Spectral analysis

The phase distortions and baseline of the resulting spectra of the eight strains were manually modified using the software TopSpin 3.6.0 (Bruker). Identification of metabolites was conducted using one-dimensional (1D) ^{1}H and 2D ^{1}H–^{13}C spectra cooperatively. The chemical shifts were verified using ChenomX NMR Suite (ChenomX Inc., Edmonton, AB, Canada), the PubChem database (https://pubchem.ncbi.nlm.nih.gov), the Madison Metabolomics Consortium Database (http://mmcd.nmrfam.wisc.edu), the Biological Magnetic Resonance Data Bank (http://www.bmrb.wisc.edu/metabolomics), the Human Metabolome Database (http://www.hmdb.ca/), and related references. Furthermore, the water (4.60–5.14) and methanol (3.28–3.33) regions were excluded from the spectra and the processed spectra (0.5–10.0 ppm) were normalized to the sum intensities. Buckets with 0.02 ppm width were obtained and the binned data were subject to multivariate analysis (Mahmud et al., 2015a).

Hierarchical cluster analysis of the bucket tables was conducted by SPSS (IBM, Armonk, NY, USA). In addition, the PCA was performed using the bucket data (Vong et al., 2018). The Euclidean distances among the variables were further calculated based on the obtained score plots of PCA. The pairwise comparisons of strains with the highest Euclidean distance were selected for further analysis of metabolic differences. The fold changes (FCs) of the identified metabolites and related *P* values in pairwise groups were calculated based on the binned data and a volcano plot was constructed (Feng et al., 2014). Metabolites with a FC $>$ 2 and $P < 0.05$ were considered as statistically significant (Mahmud et al., 2015b). The enrichment pathway analysis was then performed using MetaboAnalyst 4.0 (http://www.metaboanalyst.ca/) with the screened metabolites.

2.5. Acid response of selected strains

The acid stress-tolerances of selected strains (serotypes *E. coli* ATCC 25922 and O26:H11) were checked using *in vitro* and *in vivo* tests based on our previous work (Chen et al., 2019c). For the *in vitro* test, the bacterial pellets from 40 mL of TSB cultures were prepared as mentioned above. Moreover, the microbial cells were concentrated by resuspension in 8.5 g/L sterile saline (1 mL). The concentrated bacterial solution was then mixed well with 9 mL of lactic acid (LA, 2%, v/v final concentration, pH 2.56). During the acid treatment, 1 mL of the suspension was mixed with 2 mL neutralizing buffer (0.2 M PBS, pH 7.5) at 0, 5, 15, 30, 60, and 120 s. The obtained neutralised bacterial solutions were serially diluted and spread onto TSA for cell counting after culturing overnight at 37 °C.

For the *in vivo* test, the two strains were adapted to 100 μg/mL of nalidixic acid (Sigma-Aldrich, St. Louis, MO, USA) by several rounds of transfer with stepwise increments in the nalidixic acid concentration. Cultures (200 mL) of the two *E. coli* strains were prepared in TSB (100 μg/mL of nalidixic acid) after culturing for 18 h (37 °C). Organic broccoli sprouts (*Brassica oleracea* var. *italica*) were planted by our previous study (Chen et al., 2018a). The harvest sprouts were immersed in the prepared *E. coli* cultures for 10 min and then air-dried for 30 min. The inoculated sprouts were subsequently submerged in the LA solution (2%, v/v) for 0, 5, 15, 30, 60, and 120 s. After the sanitizing treatment, the sprouts were washed by sterile water to remove the residual LA. The broccoli sprouts (1 g) collected at each time point were ground in 6 mL

8.5 g/L sterile saline by a sterile mortar and pestle. The appropriate dilutions (0.1 mL) were spread on the TSA with 100 μg/mL of nalidixic acid. Cell counting was conducted after overnight culture at 37 °C and the results were expressed as log CFU/g fresh weight (FW) (Liu et al., 2017a). To check the different acidic tolerances of the two strains statistically, the *in vitro* and *in vivo* antibacterial effects (log CFU/mL reduction of each time point compared with the initial counts at 0 s) were fitted using the Weibull model: $N = (t/t_1)^a$, where N is the log CFU/mL (or log CFU/g FW) reduction, t is the time in s, t_1 is the time needed for 1 log CFU/mL (or log CFU/g FW) reduction, and a is the shape parameter (Chen et al., 2019c).

Morphological changes of the two *E. coli* strains under acid stress were monitored using atomic force microscope (AFM). The bacterial suspensions were prepared as mentioned in the *in vitro* study subsection. Suspensions after treatment of acid for 0 and 30 s were spread onto mica sheets and immediately dried using an aurilave (Zhang and Yang, 2017). The sheets were then air-dried in a laminar flow cabinet for 4 h and the prepared sheets were scanned using a tabletop atomic force microscope (AFM workshop, Signal Hill, CA, USA) in 4 h. The images were scanned under a 0.4 Hz scan rate for 512 scan lines (tapping mode). The offline software Gwyddion was used to analyse the obtained images and the width, height, and roughness of the cells were recorded (Chen et al., 2018b). Roughness was calculated from the central region (0.2 × 0.2 μm) of individual cell surfaces and 20 measurements were conducted for data analysis. Protein leakage of *E. coli* was tested according to a previous study (Zhao et al., 2017). The neutralised bacterial solutions at 0 and 30 s were collected and centrifuged at 12,000 × *g* for 10 min (4 °C). The protein concentration of the suspension was determined using Coomassie brilliant blue G-250 solution. The protein leakage of the selected strains was calculated as $C_{30\ s}–C_{0\ s}$.

2.6. Metabolic responses of selected strains under acidic stress

The neutralised bacterial solutions after acidic treatment for 30 s were prepared as mentioned in *in vivo* test subsection. The bacterial suspensions were centrifuged at 4500 × *g* for 10 min (24 °C) and washed twice by 0.1 M phosphate-buffered saline (PBS, pH 7.2). Extraction of the metabolites from the obtained pellets was conducted as mentioned above. NMR testing was performed under the same condition as those used for metabolic analysis of the eight *E. coli* strains. The ^{1}H spectra of two selected strains under acid stress for 30 s were processed and tested by supervised orthogonal partial least squares discriminant analysis (OPLS-DA). The R^2X and Q^2 values were applied to verify the qualities of the models. Color-coded loading and coefficient plots were obtained to illustrate the discriminated metabolites that were related to acid stress in the two *E. coli* strains (Chen et al., 2019b). Moreover, variable importance in projection (VIP) analysis was performed to identify the most influenced metabolites. The screened metabolites were subject to analysis of the related metabolic pathways in MetaboAnalyst 4.0 (http://www.metaboanalyst.ca/) and the hypothetical interpretations were concluded based on the database Kyoto Encyclopedia of Genes and Genomes (KEGG) (https://www.genome.jp/kegg/pathway.html).

2.7. Quantitative real-time PCR for selected genes

According to the biological pathways study, the expression patterns of four genes [glutamic acid decarboxylases (*GadA*, *GadB*), glutamate/γ-amino butyric acid antiporter (*GadC*), and lysine decarboxylase (*CadA*)] involved in acid stress tolerance were studied using qPCR (Lund et al., 2014). Total RNA was extracted from bacterial pellets obtained from 3 mL of neutralised bacterial solutions after acid treatment for 30 s. A Total RNA Mini-Pre Kit (Bio Basic, Ontario, Canada) was used and the qualities and concentrations of the RNA samples were tested using a spectrophotometer (BioDrop, Biochrom, Cambridge, UK). The RNA integrity was further checked using 1% (w/v) agarose gel electrophoresis, and the cDNA was synthesised. The *rrsA* gene (encoding the 16S ribosomal RNA; sense primer: 5′-CTCTTGCCATCGGATGTGCCCA-3′; antisense primer: 5′-CCAGTGTGGCTGGTCATCCTCTCA-3′) was used as the reference gene. The specific primers used in this study were obtained from previous studies (Chattopadhyay et al., 2015; Vazquez-Juarez et al., 2008). The qPCR reaction was performed according to our previous study (Chen et al., 2019a).

2.8. Statistical analysis

Data were statistically analysed with analysis of variance (ANOVA), and the least significant difference method was applied to compare the means. Differences with a P value < 0.05 were regarded as statistically significant.

3. Results and discussion

3.1. Identification and comparison of metabolites in E. coli strains

E. coli ATCC 25922 is extensively applied in food microbiology studies as a surrogate for pathogenic serotypes, and O157:H7 is one of the most prominent Shiga toxigenic foodborne pathogens (Kanankege et al., 2017). Thus, the metabolic differences among *E. coli* ATCC 25922, typical strains from serotypes of O157: H7 and “big six” were studied in this work. The metabolic spectra of eight *E. coli* strains [I: ATCC 25922; II: O157:H7 (ATCC 43895); III: O103:H11 (ATCC BAA-2215); IV: O26:H11 (ATCC BAA-2196); V: O145 (ATCC BAA-2192); VI: O121:H19 (ATCC BAA-2219); VII: O45:H2 (ATCC BAA-2193); VIII: O111 (ATCC BAA-2440)] are shown in Fig. 1. Multiple ^{1}H peaks were located in the region of 0.5–10 ppm. Most of the signals in the eight spectra were recorded in around 0.5–5 ppm. Aliphatic acids and sugars are designated to this range (Chen et al., 2019b). Nucleoside derivatives assigned at around 4.0–4.5 ppm were also observed (Planchon et al., 2017). The signals located in the 5–10 ppm region represented other metabolites, including nucleotides and sugars (Liu et al., 2017b). In addition, based on two representative 2D ^{1}H–^{13}C spectra of representative *E. coli* samples, a total of 38 metabolites were identified (Fig. 1; Table S1). Various amino acids (e.g., valine, arginine, lysine, and glutamic acid) and sugars (e.g., β-D-glucose, and glucose-1-phosphate) were detected. Moreover, multiple nucleotide assignments, such as ATP, cyclic AMP, ADP, and NADP, were recorded. The results were in accordance with a previous metabolic study of *E. coli* K-12 in that the dominant intracellular metabolites were amino acids, nucleotides, and central carbon intermediates (Bennett et al., 2009).

Furthermore, the 1D ^{1}H spectra results showed that metabolic diversity existed among the eight strains. *E. coli* ATCC 25922 showed some differences in the featured ^{1}H signals compared with those for the pathogenic STECs. For example, peaks with high intensities at around 8.20 and 8.32 ppm were recorded in sample I (*E. coli* ATCC 25922) and were assigned as adenosine. The peaks located at around 8.20 and 8.48 ppm were identified as ATP, which presented higher intensities in the seven pathogenic STECs compared with that in ATCC 25922 (Fig. 1). As the most important metabolic activity, energy production is crucial for the physiological functions of *E. coli*, such as proliferation (Orth et al., 2011). The results implied that the pathogenic STECs might require a higher amount of energy for their cellular activities compared with non-pathogenic *E. coli*. Furthermore, signal differences of intracellular metabolites were also observed among the seven selected STECs (Fig. 1). For instance, the ^{1}H signal at 5.47 ppm, which was identified as glucose-1-phosphate, was detected in the spectra of four strains (IV, V, VI, and VII), while it was not detectable in the other three pathogenic strains (II, III, and VIII). This indicated that the energy metabolism may be different among STECs. *E. coli* have evolved to utilise diverse carbon and energy sources under different environments and thus individual strains present characteristic sugar and energy metabolisms (Fabich et al., 2008).

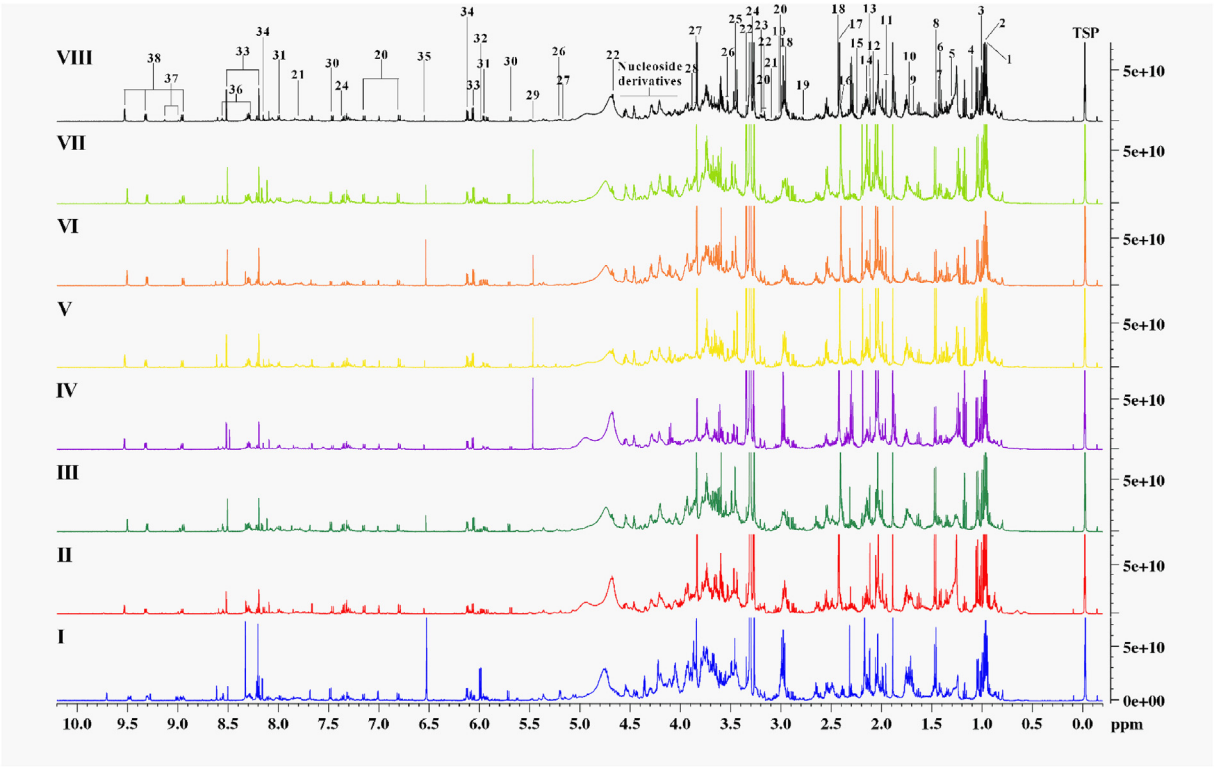

Fig. 1. ^{1}H nuclear magnetic resonance spectra of eight *E. coli* strains. Note: I, ATCC 25922; II, O157:H7; III, O103:H11; IV, O26:H11; V, O145; VI, O121:H19; VII, O45:H2; VIII, O111; TSP, trimethylsilylpropanoic acid.

3.2. Multivariate analysis

Based on the binned dataset from the ^{1}H spectra, hierarchical clustering analysis was performed (Fig. 2A). The metabolic patterns of the eight *E. coli* strains were separated into two major clusters (C1 and C2). Two subgroups (C1a and C1b) of C1 were also recorded. C1a comprised *E. coli* ATCC 25922 (I) and O157:H7 (II). C1b showed similarities between O103:H11 (III) and O111 (VIII). The cluster distribution of C2 was different to that of C1. Strain O26:H11 (IV) was distinguished from the other three strains and O145 (V) and O45:H2 (VII) exhibited relative higher similarities. A previous study showed that of the five surrogates of *E. coli* O157:H7, *E. coli* ATCC 25922 presented the most similar cell surface characteristics and attachment ability (Kim and Harrison, 2009). Our results further verified their similarities at the metabolic level. The molecular profiles of the STECs revealed a high level of genetic diversity among serotypes, which might contribute to the various metabolic characteristics (Balière et al., 2016).

PCA is a useful tool to screen the principal metabolites from high throughput profiles. In the present study, the separation of variables was analysed and the discriminative metabolites were highlighted using PCA. The first five principal components (PCs) explained 89.1% of the total data (PC1: 32.5%; PC2: 25.1%; PC3: 15.0%; PC4: 9.5%; PC5: 7.2%) and the Q^2 value (0.65 $>$ 0.5) indicated the good model prediction (Fig. 2B). The score plot exhibited the well separations of the eight groups (Fig. 2C). Moreover, the loading plots (Fig. 2D) presented the discriminative metabolites for the separated variables. For example, group I was negatively affected by PC1 and PC2 (Tables S2 and S3). Metabolites including lysine, arginine, α-ketoglutaric acid, adenosine, and fumaric acid were closely related to group I (Tables S4 and S5). In addition, group VII, which was characterised by proline, pyruvic acid, and α-D-glucose, was positively related to PC2 and PC5 (Tables S2–S5).

The increasing availability of genomic sequences of different *E. coli* serotypes has revealed their genomic diversity. For instance, the genome of the extensively used model organism *E. coli* K-12 is around 20% smaller than that of *E. coli* O157:H7. However, genome annotation does not provide an understanding of the integrated function of gene products (Monk et al., 2013). The PCA of metabolic differences of STEC strains from different serotypes in the present study revealed the metabolic diversity. The reuslts may reveal core sets of metabolic capabilities of STECs and further provide new insights to prevent and control STEC infections.

The Euclidean distances of pairwise variables were calculated based on the PCA score plot (Fig. 2E). The results showed Euclidean distances ranging from 15.18 to 53.81 among the eight strains. Group I generally showed long Euclidean distances compared with the other groups. The results implied large metabolic differences between non-pathogenic and pathogenic *E. coli* strains. Similarly, Monk et al. (2013) observed significantly different metabolic capabilities between non-pathogenic *E. coli* K12 and pathogenic (both extraintestinal and intestinal) serotypes based on simulated growth phenotypes. Furthermore, the highest Euclidean distance, 53.81, was observed between group I (ATCC 25922) and IV (O26:H11) (Fig. 2E), indicating their notable metabolic differences. Moreover, a previous study of virulence-associated gene targets in 28 STEC and 75 enteropathogenic *E. coli* strain showed that the O26:H11 was associated with a large number of virulence-associated genes (Balière et al., 2016). Thus, the pairwise metabolic differences of groups I-IV were further studied.

3.3. Metabolic difference between E. coli ATCC 25922 and O26:H11

The fold changes of identified metabolites between *E. coli* ATCC 25922 and O26:H11 were calculated based on the relative contents obtained from the ^{1}H spectra (Fig. 3A). Among the 28 compounds without overlapping shifts, the contents of 13 metabolites were significantly different, by more than 2 fold (P $<$ 0.05) between the two strains. Moreover, metabolites including ATP, pyruvic acid, glucose-1-phosphate, and succinic acid in O26:H11 were present at 3.55–56.17 times higher levels than those in strain ATCC 25922 (Fig. 3A and B). By

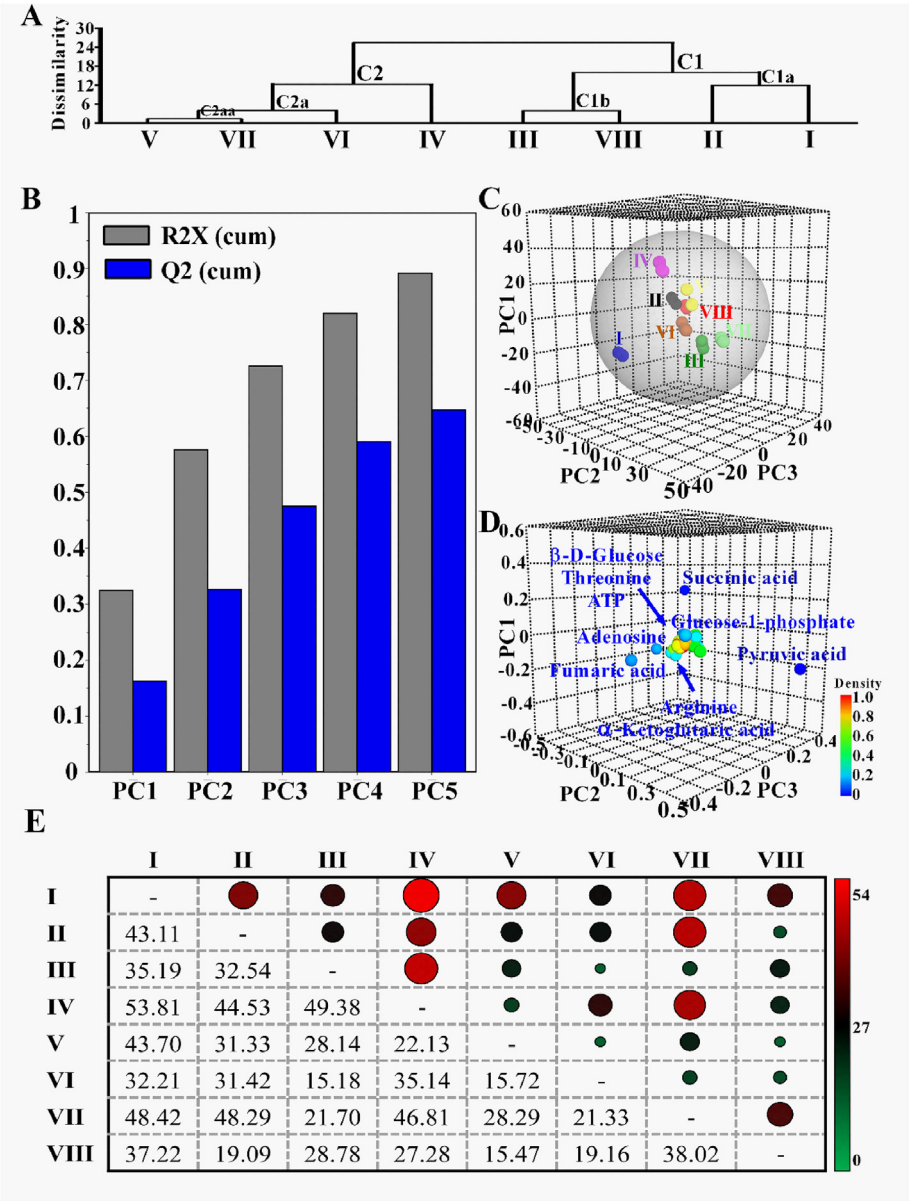

Fig. 2. Hierarchical cluster analysis of eight strains (A). The principal components explaining variances used in principal component analysis (PCA) (B). The 3D score plots of PCA (C). The 3D loading plot of PCA (D). Euclidean distances among the eight variables (E).

contrast, higher relative contents of α-ketoglutaric acid, arginine, histidine, phenylalanine, lysine, adenosine, ADP, NADP, and uracil were recorded in ATCC 25922. This indicated that under a rich-nutritive environment, pathogenic *E. coli* O26:H11 might have a higher tricarboxylic acid (TCA) cycle rate and require higher levels of ATP to maintain its physiological activities. It has been proposed that gluconeogenesis and the TCA cycle are essential when *E. coli* infects the urinary tract (Fuchs et al., 2012). The requirement of host infection ability might result in the higher energy requirement of pathogenic serotypes. The higher proportions of metabolites such as amino acids in *E. coli* ATCC 25922 serve as substrates for nutritive growth (Dai et al., 2011).

To further study the metabolic pathway differences, metabolite-based enrichment pathway analysis was conduced and the results are shown in Fig. 3C and D. The screened metabolites in group I and IV were subject to MetaboAnalyst 4.0 analysis. Of the fifty analysed metabolic sets in strain I, ten (β-alanine metabolism, arginine and proline metabolism, phytanic acid peroxisomal oxidation, urea cycle, lysine degradation, ammonia recycling, histidine metabolism, glucose-alanine cycle, glutamate metabolism, and alanine metabolism) were recognised as the significant sets, with $P < 0.01$ (Table S6). Moreover, group IV was characterised by 19 metabolic sets, such as glycolysis, the TCA cycle, and gluconeogenesis (Table S7). The results further confirmed our hypothesis that pathogenic O26:H11 might require higher energy production to fuel its physiological activities compared with those in the non-pathogenic strain ATCC 25922.

3.4. Acid responses of selected E. coli strains

Although *E. coli* ATCC 25922 is extensively applied in food microbiology as a surrogate of pathogenic *E. coli* serotypes because of their similar physiological characteristics (Liu et al., 2017b; Zhao et al., 2017; Zhao et al., 2019a), increasing evidence suggests that *E. coli* serotypes present different responses to sanitizing stresses. For example, *E. coli* ATCC 25922 and K-12, which show higher sensitivity to pulsed electric field treatment, were not considered as valid surrogates for either *Salmonella* or *E. coli* O157:H7 (Gurtler et al., 2010). Our data revealed a wide metabolic diversity among *E. coli* strains from different

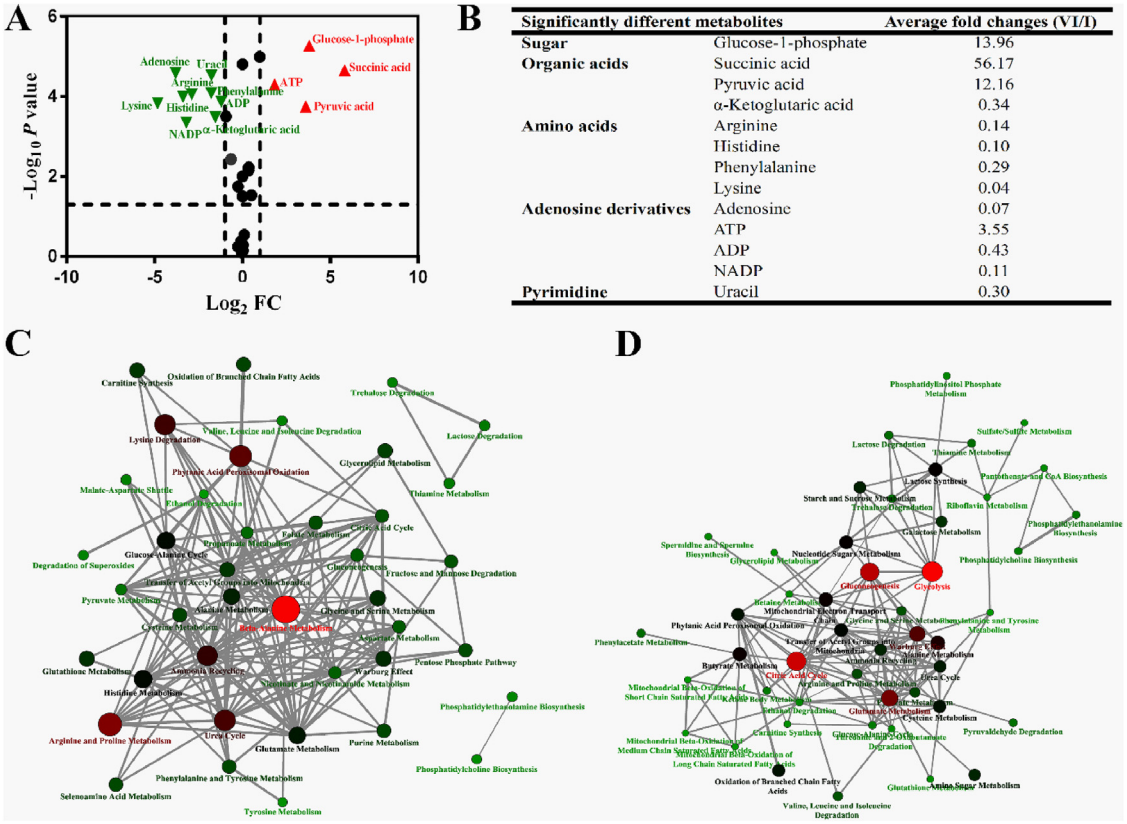

Significantly different metabolites		Average fold changes (VI/I)
Sugar	Glucose-1-phosphate	13.96
Organic acids	Succinic acid	56.17
	Pyruvic acid	12.16
	α-Ketoglutaric acid	0.34
Amino acids	Arginine	0.14
	Histidine	0.10
	Phenylalanine	0.29
	Lysine	0.04
Adenosine derivatives	Adenosine	0.07
	ATP	3.55
	ADP	0.43
	NADP	0.11
Pyrimidine	Uracil	0.30

Fig. 3. Volcano plots of screened metabolites in *E. coli* ATCC 25922 (I) and O26:H11 (IV); the red ▲ symbol indicates metabolites with higher relative contents in O26:H11, while the green ▼ symbol indicates metabolites with higher relative contents in ATCC 25922 (A). Average fold changes of screened metabolites (O26:H11/ATCC 25922) (B). Enrichment pathway analysis of *E. coli* ATCC 25922 based on screened metabolites (C). Enrichment pathway analysis of *E. coli* O26:H11 based on screened metabolites (D). Note: for C and D, nodes represent –log(P) values of metabolic sets and edges represent the interaction between two sets. (For interpretation of the references to color in this figure legend, the reader is referred to the Web version of this article.)

serotypes, suggesting that they might show different stress responsess. An acidic environment is a common stress factor in the food industry. Our previous work showed the inactivation effect of lactic acid (LA, 2%, v/v) on *Listeria* under *in vitro* and *in vivo* conditions (Chen et al., 2019c). In the present study, the basic physiological characteristics of selected *E. coli* strains under LA treatment were compared. The different metabolic responses of the strains were further tested using NMR.

The acid tolerances of *E. coli* ATCC 25922 (I) and O26:H11 (IV) were assessed and the *in vitro* results showed that group I was more sensitive than group IV under the first 15 s of acidic stress (Fig. 4A). Weibull fitting showed that the time needed for a 1 log CFU/mL reduction of strain I (2.05 s) was significantly less than that of strain IV (8.45 s). Similar results were found for two *E. coli* strains inoculated in organic broccoli sprouts (Fig. 4B). It took longer to reach a 1 log CFU/g fresh weight (FW) reduction for strain IV. The results indicated that the pathogenic *E. coli* O26:H11 was more acid-tolerant compared with non-pathogenic ATCC 25922. King et al. (2010) suggested that pathogenic *E. coli* serotypes possessed additional molecular mechanisms contributing to acid resistance and that they might have greater abilities to survive under more complex acidic environments in hosts or during food processing.

The morphologies of the two *E. coli* strains under acid stress were monitored using AFM (Fig. 4C–G). The images revealed adhered bacterial cells in each group. Rod-shaped *E. coli* ATCC 25922 (I) cells (width: 0.64 μm; height: 0.17 μm) with rough outer membranes (3.18 nm) were observed. Moreover, Fig. 4D shows larger O26:H11 cells (width: 1.46 μm; height: 0.24 μm) with a surface roughness of 2.53 nm. After 30 s of LA treatment, the cell width of strain I increased to 1.19 μm. However, the height and roughness decreased significantly ($P < 0.05$) to 0.11 μm and 1.75 nm, respectively. By contrast, the cell morphology of strain IV mostly maintained after acid treatment. Gram-negative *E. coli* cells are covered by a thick outer membrane of lipopolysaccharide, which represents a barrier for stresses (Liu and Yang, 2019; Putker et al., 2015). The AFM results indicated that the acid treatment might destroy the outer membrane structure, resulting in the emergence of the smooth cytoplasmic membrane. Moreover, the bacterial cells (in group I) had collapsed without the structural support of the outer membrane. However, acid treatment caused less damage to the membrane of pathogenic strain IV than to that of strain I. This observation was supported by the protein leakage results (Fig. 4H). The leakage of cytoplasmic proteins indicates structural changes of the outer membrane (Liu et al., 2018). A previous study reported that organic acid inactivates bacteria via enhancing the membrane permeability (Wang et al., 2013). Compared with the leakage from strain IV (20.60 μg/mL), significantly higher protein leakage (54.35 μg/mL; $P < 0.01$) was observed from strain I cells, indicating more severe membrane damage to strain I.

3.5. Alterative metabolites of selected strains under acidic stress

The metabolic spectra of the two selected strains under acid stress are shown in Fig. 5A. The binned data were obtained and subject to supervised OPLS-DA. PC1 was the dominated component (R^2: 0.99) to separate the two groups (Fig. 5B). Also, the high Q^2 value (0.99) revealed good-fitness of the model. The extracted loading S-line presented discriminative metabolites of the two groups. The metabolic peaks that point upwards indicate higher relative contents in group I, while the downward peaks indicate higher relative contents in IV (Fig. 5C). In addition, the red color of most of the peaks implied significant metabolic differences between the two groups. The coefficient plots shown

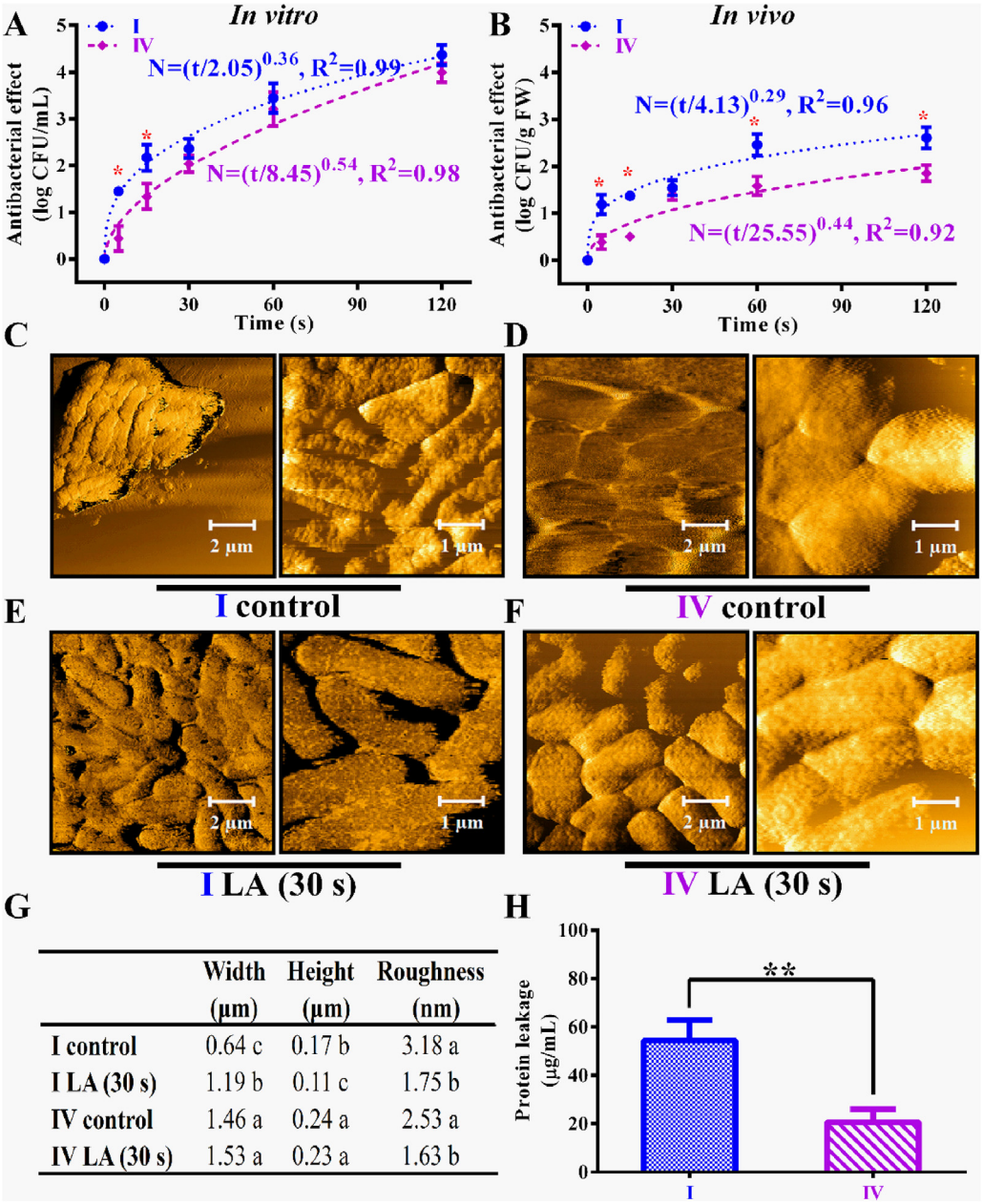

	Width (μm)	Height (μm)	Roughness (nm)
I control	0.64 c	0.17 b	3.18 a
I LA (30 s)	1.19 b	0.11 c	1.75 b
IV control	1.46 a	0.24 a	2.53 a
IV LA (30 s)	1.53 a	0.23 a	1.63 b

Fig. 4. *In vitro* antibacterial effect of lactic acid on *E. coli* ATCC 25922 (I) and O26:H11 (IV) (A). *In vivo* antibacterial effect of lactic acid on stains I and IV (B). Nanostructure of strain I before lactic acid treatment (C). Nanostructure of strain IV before lactic acid treatment (D). Nanostructure of strain I after lactic acid treatment for 30 s (E). Nanostructure of strain IV after lactic acid treatment for 30 s (F). Statistical parameters of *E. coli* cells (G). Protein leakage of two strains after acid treatment for 30 s (H). Note: the symbol * indicates a significant difference ($P < 0.05$), ** indicates a very significant difference ($P < 0.01$).

in Fig. 5D statistically summarise the discriminative metabolites between I and IV. Of the 28 quantified metabolites, 11 metabolites, including pyruvic acid, α-D-glucose, proline, aspartic acid, arginine, isoleucine, glucose-1-phosphate, succinic acid, phenylalanine, NADP, and glutamic acid showed higher contents in group I. Higher levels of the remaining 17 compounds were recorded in IV. Metabolites with a VIP > 0.5 and $P < 0.05$ were selected as statistically significant compounds. Thus, α-D-glucose, pyruvic acid, and proline were the featured metabolites for group I. For strain IV, there were 7 significant factors (adenosine, lysine, uracil, α-ketoglutaric acid, uridine, NAD, γ-aminobutyric acid) for pair-wise discrimination (Fig. 5D).

Pathway analysis was performed to screen the most relevant pathways involved in the acid responses of the two strains, based on the selected discriminative metabolites. Pathways showing $P < 0.05$ (arginine and proline metabolism; alanine, aspartate and glutamate metabolism; butanoate metabolism; citrate cycle; glycolysis or gluconeogenesis; biphenyl degradation; carbazole degradation) were considered as significant metabolic pathways (Fig. 5E, Table S8). Based on the discriminated metabolites, pathway, KEGG, and MetaboAnalyst 4.0 database analyses, the hypothesised different biochemical responses of the two *E. coli* strains under acid stress are shown in Fig. 5F. Higher contents of TCA cycle related metabolites revealed more active TCA activity in strain IV. The results were in accordance with metabolic differences of the two strains under normal culture conditions (Fig. 3D). In addition, compared with that in strain I, strain IV (O26:H11) presented more complex mechanisms, such as amino acid and purine metabolisms. For *E. coli*, mechanisms including F_1–F_0 ATPase, amino acid-dependent decarboxylase/antiporter system, deiminase and deaminase systems, are involved in survival in acidic environments (Lund et al., 2014). Protons can be actively pumped out to the extracellular

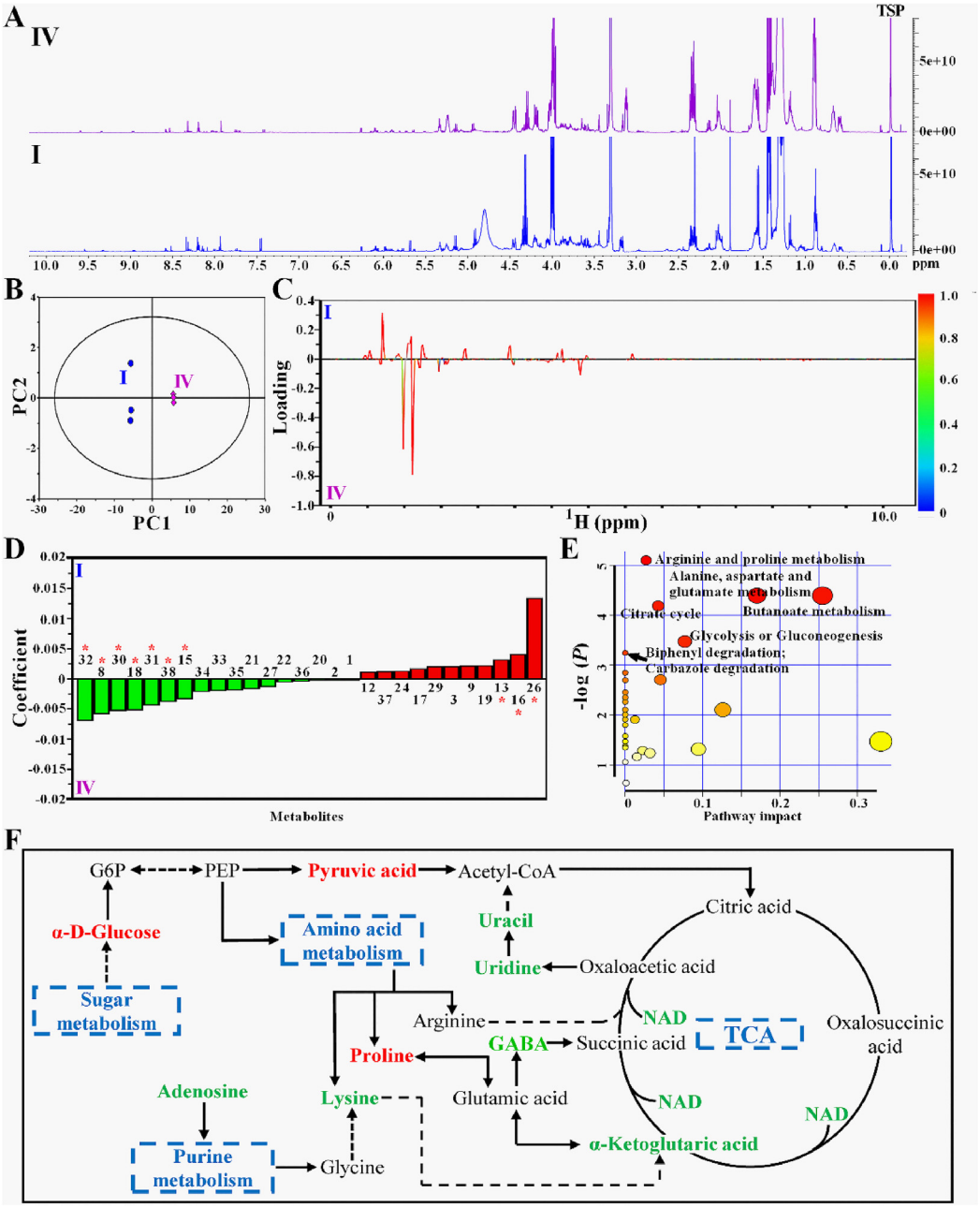

Fig. 5. ^{1}H spectra of *E. coli* ATCC 25922 (I) and O26:H11 (IV) after lactic acid treatment for 30 s (A). Orthogonal partial least squares discriminant analysis (OPLS-DA) score plot of group I and IV, $R^2 = 0.99$, $Q^2 = 0.99$ (B). OPLS-DA loading S-line (C). Coefficient plot of group I and IV; metabolites marked with * indicate a significant contribution to the OPLS-DA models (VIP $>$ 0.5, $P < 0.05$) (D). Overview of the pathway analysis of group I and IV (E). Biochemical pathway analysis of acidic responses of selected strains; metabolites colored in red and green represent higher relative contents in I and IV, respectively (F). (For interpretation of the references to color in this figure legend, the reader is referred to the Web version of this article.)

space using energy provided by ATPase. A non-significantly higher ATP content was recorded in pathogenic strain IV (Fig. 5D), indicating that O26:H11 could utilise more energy for proton pumping.

Amino acid metabolism was screened as the most influenced pathway between I and IV under acidic stress (Fig. 5E, Table S8). Higher levels of amino acid and related derivatives, such as lysine and γ-aminobutyric acid (GABA) were observed in strain IV (Fig. 5D, F). Indeed, glutamic acid, lysine, and arginine-dependent decarboxylase/antiporter systems are the major anti-acid mechanisms in *E. coli*. Intracellular protons can be consumed via biochemical reactions catalysed by amino acid decarboxylases (Lund et al., 2014). For example, cytoplasmic protons are bound to carbon atoms of glutamic acid by GadA and GadB to produce GABA. The generated GABA is then exchanged with extracellular glutamic acid through the activity of GadC (Ma et al., 2013). The higher contents of lysine and GABA in strain IV indicated that amino acid metabolism might contribute to the enhanced acid resistance of pathogenic O26:H11.

3.6. Expression patterns of selected genes

To further understand and confirm the hypothesis that amino acid metabolism might contribute to the enhanced acid resistance of pathogenic O26:H11, the expression levels of acid resistance-related genes, including *GadA*, *GadB*, *GadC*, and *CadA*, were checked using qPCR. CadA catalyses lysine and proton to produce cadaverine (He et al., 2017). The results indicated that, under acid stress, the

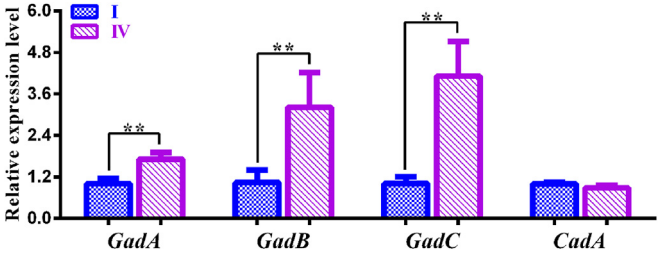

Fig. 6. Relative expression of acid tolerance related genes. Note: *GadA*, *GadB*, glutamic acid decarboxylases; *GadC*, glutamate/γ-amino butyric acid antiporter; *CadA*, lysine decarboxylase. Note: the symbol ** indicates a very significant difference ($P < 0.01$).

expression levels of three genes from the glutamic acid dependent decarboxylase/antiporter system (GadA, GadB, and GadC) in strain VI were 1.71–4.11 folds ($P < 0.01$) higher than those in strain I. However, no significant differences in *CadA* expression were observed between strains I and IV. The results suggested that although lysine was enriched in strain IV during the acid response, the glutamic acid dependent decarboxylase/antiporter system was the major pathway related to the acid resistance mechanism of O26:H11. This conclusion agreed with those of previous studies (He et al., 2017; Moreau, 2007). Different amino acid-dependent decarboxylases are characterised by different pH ranges for induction and proton consumption. CadA is thought to be ineffective in *E. coli* at pH 2.5, but peaks at around pH 6.0. Furthermore, the glutamic acid-dependent system is by far the most effective acid resistance mechanism in *E. coli* (Lund et al., 2014). The characteristic metabolites (Fig. 5) and gene expression levels (Fig. 6) suggested that the different metabolic responses might contribute to the different stress tolerances of *E. coli* strains.

4. Conclusion

This study investigated the metabolic diversity of *E. coli* strains from different serotypes using NMR. Based on the observed metabolic differences, the acid responses of selected strains were further tested. Among the eight tested *E. coli* strains, the non-pathogenic strain ATCC 25922 was characterised by lysine, arginine, α-ketoglutaric acid, adenosine, and fumaric acid, and presented relatively large differences in intracellular metabolism compared with the pathogenic strains. Further enrichment analysis of pairwise strains (ATCC 25922 and O26:H11) with the greatest Euclidean distance showed that the pathogenic O26:H11, which was characterised by glycolysis, gluconeogenesis, and TCA cycle metabolism sets, might require higher energy production for its physiological activities. The acid tolerances of the two strains were assessed using *in vitro* and in *vivo* inactivation effects, morphological changes, and protein leakage. *E. coli* O26:H11 presented higher acid resistance compared with that of ATCC 25922 and the different amino acid metabolic responses between the two strains might contribute to this difference. qPCR of selected genes confirmed the hypothesis that O26:H11 possessed a more effective glutamic acid dependent decarboxylase/antiporter system compared with that in non-pathogenic ATCC 25922. The results also implied more cautious uses of surrogates of *E. coli* serotypes such “big six” for certain metabolic and stress-treated studies.

Declaration of competing interest

We declare that we do not have any commercial or associative interest that represents a conflict of interest in connection with this manuscript. We have no financial and personal relationships with other people or organisations that can inappropriately influence our work.

Acknowledgement

This study was funded by the Singapore Ministry of Education Academic Research Fund Tier 1 (R-143-000-A40-114), Natural Science Foundation of Jiangsu Province (BK20181184), and an industry grant supported by Shanghai ProfLeader Biotech Co., Ltd (R-143-000-A21-597).

Appendix A. Supplementary data

Supplementary data to this article can be found online at https://doi.org/10.1016/j.fm.2019.103399.

References

Ås, C.G., Drabløs, F., Haugum, K., Afset, J.E., 2018. Comparative transcriptome profiling reveals a potential role of type VI secretion system and fimbriae in virulence of non-O157 Shiga toxin-producing *Escherichia coli*. Front. Microbiol. 9, 1416.
Balière, C., Rincé, A., Delannoy, S., Fach, P., Gourmelon, M., 2016. Molecular profiling of Shiga toxin-producing *Escherichia coli* and enteropathogenic *E. coli* strains isolated from French coastal environments. Appl. Environ. Microbiol. 82 (13), 3913–3927.
Bennett, B.D., Kimball, E.H., Gao, M., Osterhout, R., Van Dien, S.J., Rabinowitz, J.D., 2009. Absolute metabolite concentrations and implied enzyme active site occupancy in *Escherichia coli*. Nat. Chem. Biol. 5 (8), 593.
Chattopadhyay, M.K., Keembiyehetty, C.N., Chen, W., Tabor, H., 2015. Polyamines stimulate the level of the σ38 subunit (RpoS) of *Escherichia coli* RNA polymerase, resulting in the induction of the glutamate decarboxylase-dependent acid response system via the gadE regulon. J. Biol. Chem. 290 (29), 17809–17821.
Chen, L., Tan, G.J.T., Pang, X., Yuan, W., Lai, S., Yang, H., 2018a. Energy regulated nutritive and antioxidant properties during the germination and sprouting of broccoli sprouts (*Brassica oleracea* var. *italica*). J. Agric. Food Chem. 66 (27), 6975–6985.
Chen, L., Tan, J.T.G., Zhao, X., Yang, D., Yang, H., 2019a. Energy regulated enzyme and non-enzyme-based antioxidant properties of harvested organic mung bean sprouts (*Vigna radiata*). LWT-Food Sci. Technol. 107, 228–235.
Chen, L., Wu, J.E., Li, Z., Liu, Q., Zhao, X., Yang, H., 2019b. Metabolomic analysis of energy regulated germination and sprouting of organic mung bean (*Vigna radiata*) using NMR spectroscopy. Food Chem. 286, 87–97.
Chen, L., Zhang, H., Liu, Q., Pang, X., Zhao, X., Yang, H., 2019c. Sanitising efficacy of lactic acid combined with low-concentration sodium hypochlorite on *Listeria innocua* in organic broccoli sprouts. Int. J. Food Microbiol. 295, 41–48.
Chen, L., Zhao, X., Wu, J.E., He, Y., Yang, H., 2020. Metabolic analysis of salicylic acid-induced chilling tolerance of banana using NMR. Food Res. Int. 128, 108796.
Chen, L., Zhou, Y., He, Z., Liu, Q., Lai, S., Yang, H., 2018b. Effect of exogenous ATP on the postharvest properties and pectin degradation of mung bean sprouts (*Vigna radiata*). Food Chem. 251, 9–17.
Dai, Z.L., Wu, G., Zhu, W.Y., 2011. Amino acid metabolism in intestinal bacteria: links between gut ecology and host health. Front. Biosci. 16 (1), 1768–1786.
Diodati, M., Bates, A., Miller, W., Carter, M., Zhou, Y., Brandl, M., 2016. The polymorphic aggregative phenotype of Shiga toxin-producing *Escherichia coli* O111 depends on RpoS and curli. Appl. Environ. Microbiol. 82 (5), 1475–1485.
Fabich, A.J., Jones, S.A., Chowdhury, F.Z., Cernosek, A., Anderson, A., Smalley, D., McHargue, J.W., Hightower, G.A., Smith, J.T., Autieri, S.M., 2008. Comparison of carbon nutrition for pathogenic and commensal *Escherichia coli* strains in the mouse intestine. Infect. Immun. 76 (3), 1143–1152.
Feng, J., Ma, L., Nie, J., Konkel, M.E., Lu, X., 2018. Environmental stress-induced bacterial lysis and extracellular DNA release contribute to *Campylobacter jejuni* biofilm formation. Appl. Environ. Microbiol. 84 (5) e02068-02017.
Feng, S., Eucker, T.P., Holly, M.K., Konkel, M.E., Lu, X., Wang, S., 2014. Investigating the responses of *Cronobacter sakazakii* to garlic-drived organosulfur compounds: a systematic study of pathogenic-bacterium injury by use of high-throughput whole-transcriptome sequencing and confocal micro-Raman spectroscopy. Appl. Environ. Microbiol. 80 (3), 959–971.
Fuchs, T.M., Eisenreich, W., Heesemann, J., Goebel, W., 2012. Metabolic adaptation of human pathogenic and related nonpathogenic bacteria to extra-and intracellular habitats. FEMS (Fed. Eur. Microbiol. Soc.) Microbiol. Rev. 36 (2), 435–462.
Gómez-Aldapa, C.A., Segovia-Cruz, J.A., Cerna-Cortes, J.F., Rangel-Vargas, E., Salas-Rangel, L.P., Gutiérrez-Alcántara, E.J., Castro-Rosas, J., 2016. Prevalence and behavior of multidrug-resistant shiga toxin-producing *Escherichia coli*, enteropathogenic *E. coli* and enterotoxigenic *E. coli* on coriander. Food Microbiol. 59, 97–103.
Gurtler, J.B., Rivera, R.B., Zhang, H.Q., Geveke, D.J., 2010. Selection of surrogate bacteria in place of *E. coli* O157: H7 and *Salmonella Typhimurium* for pulsed electric field treatment of orange juice. Int. J. Food Microbiol. 139 (1–2), 1–8.
Han, D., Hung, Y.C., Bratcher, C.L., Monu, E.A., Wang, Y., Wang, L., 2018. Formation of sublethally injured *Yersinia enterocolitica, Escherichia coli* O157: H7, and *Salmonella enterica* serovar enteritidis cells after neutral electrolyzed oxidizing water treatments. Appl. Environ. Microbiol. 84 (17) e01066-01018.
He, A., Penix, S.R., Basting, P.J., Griffith, J.M., Creamer, K.E., Camperchioli, D., Clark, M.W., Gonzales, A.S., Erazo, J.S.C., George, N.S., 2017. Acid Evolution Deletes Amino-Acid Decarboxylases and Reregulates Catabolism of *Escherichia coli* K-12. Applied and Environmental Microbiology AEM. 00442-00417.
Hsu, H., Sheen, S., Sites, J., Cassidy, J., Scullen, B., Sommers, C., 2015. Effect of high

pressure processing on the survival of shiga toxin-producing *Escherichia coli* (Big Six vs. O157: H7) in ground beef. Food Microbiol. 48, 1–7.
Kanankege, K.S., Anklam, K.S., Fick, C.M., Kulow, M.J., Kaspar, C.W., Ingham, B.H., Milkowski, A., Döpfer, D., 2017. Evaluating the efficacy of beef slaughter line interventions by quantifying the six major non-O157 Shiga toxin producing *Escherichia coli* serogroups using real-time multiplex PCR. Food Microbiol. 63, 228–238.
Kim, J.K., Harrison, M.A., 2009. Surrogate selection for *Escherichia coli* O157: H7 based on cryotolerance and attachment to romaine lettuce. J. Food Prot. 72 (7), 1385–1391.
King, T., Lucchini, S., Hinton, J.C., Gobius, K., 2010. Transcriptomic analysis of *Escherichia coli* O157: H7 and K-12 cultures exposed to inorganic and organic acids in stationary phase reveals acidulant-and strain-specific acid tolerance responses. Appl. Environ. Microbiol. 76 (19), 6514–6528.
Liu, Q., Jin, X., Feng, X., Yang, H., Fu, C., 2019. Inactivation kinetics of *Escherichia coli* O157:H7 and *Salmonella* Typhimurium on organic carrot (*Daucus carota* L.) treated with low concentration electrolyzed water combined with short-time heat treatment. Food Control 106, 106702.
Liu, Q., Tan, C.S.C., Yang, H., Wang, S., 2017a. Treatment with low-concentration acidic electrolysed water combined with mild heat to sanitise fresh organic broccoli (*Brassica oleracea*). LWT-Food Sci. Technol. 79, 594–600.
Liu, Q., Wu, J.E., Lim, Z.Y., Aggarwal, A., Yang, H., Wang, S., 2017b. Evaluation of the metabolic response of *Escherichia coli* to electrolysed water by ^{1}H NMR spectroscopy. LWT-Food Sci. Technol. 79, 428–436.
Liu, Q., Wu, J.E., Lim, Z.Y., Lai, S., Lee, N., Yang, H., 2018. Metabolite profiling of *Listeria innocua* for unravelling the inactivation mechanism of electrolysed water by nuclear magnetic resonance spectroscopy. Int. J. Food Microbiol. 271, 24–32.
Liu, Q., Yang, H., 2019. Application of atomic force microscopy in food microorganisms. Trends Food Sci. Technol. 87, 73–83.
Lund, P., Tramonti, A., De Biase, D., 2014. Coping with low pH: molecular strategies in neutralophilic bacteria. FEMS (Fed. Eur. Microbiol. Soc.) Microbiol. Rev. 38 (6), 1091–1125.
Ma, D., Lu, P., Shi, Y., 2013. Substrate selectivity of the acid-activated glutamate/γ-aminobutyric acid (GABA) antiporter GadC from *Escherichia coli*. J. Biol. Chem. 288 (21), 15148–15153.
Mahmud, I., Kousik, C., Hassell, R., Chowdhury, K., Boroujerdi, A.F., 2015a. NMR spectroscopy identifies metabolites translocated from powdery mildew resistant rootstocks to susceptible watermelon scions. J. Agric. Food Chem. 63 (36), 8083–8091.
Mahmud, I., Shrestha, B., Boroujerdi, A., Chowdhury, K., 2015b. NMR-based metabolomics profile comparisons to distinguish between embryogenic and non-embryogenic callus tissue of sugarcane at the biochemical level. In Vitro Cell. Dev. Biol. Plant 51 (3), 340–349.
McAllister, L.J., Bent, S.J., Petty, N.K., Skippington, E., Beatson, S.A., Paton, J.C., Paton, A.W., 2016. Genomic comparison of two O111: H− enterohemorrhagic *Escherichia coli* isolates from a historic hemolytic-uremic syndrome outbreak in Australia. Infect. Immun. 84 (3), 775–781.
Monk, J.M., Charusanti, P., Aziz, R.K., Lerman, J.A., Premyodhin, N., Orth, J.D., Feist, A.M., Palsson, B.Ø., 2013. Genome-scale metabolic reconstructions of multiple *Escherichia coli* strains highlight strain-specific adaptations to nutritional environments. Proc. Natl. Acad. Sci. 110 (50), 20338–20343.
Moreau, P.L., 2007. The lysine decarboxylase CadA protects *Escherichia coli* starved of phosphate against fermentation acids. J. Bacteriol. 189 (6), 2249–2261.
Orth, J.D., Conrad, T.M., Na, J., Lerman, J.A., Nam, H., Feist, A.M., Palsson, B.Ø., 2011. A comprehensive genome-scale reconstruction of *Escherichia coli* metabolism—2011. Mol. Syst. Biol. 7 (1), 535.
Planchon, M., Léger, T., Spalla, O., Huber, G., Ferrari, R., 2017. Metabolomic and proteomic investigations of impacts of titanium dioxide nanoparticles on *Escherichia coli*. PLoS One 12 (6), e0178437.
Putker, F., Bos, M.P., Tommassen, J., 2015. Transport of lipopolysaccharide to the Gram-negative bacterial cell surface. FEMS (Fed. Eur. Microbiol. Soc.) Microbiol. Rev. 39 (6), 985–1002.
Sheen, S., Cassidy, J., Scullen, B., Sommers, C., 2015. Inactivation of a diverse set of shiga toxin-producing *Escherichia coli* in ground beef by high pressure processing. Food Microbiol. 52, 84–87.
Tomat, D., Casabonne, C., Aquili, V., Balagué, C., Quiberoni, A., 2018. Evaluation of a novel cocktail of six lytic bacteriophages against Shiga toxin-producing *Escherichia coli* in broth, milk and meat. Food Microbiol. 76, 434–442.
Vazquez-Juarez, R.C., Kuriakose, J.A., Rasko, D.A., Ritchie, J.M., Kendall, M.M., Slater, T.M., Sinha, M., Luxon, B.A., Popov, V.L., Waldor, M.K., 2008. CadA negatively regulates *Escherichia coli* O157: H7 adherence and intestinal colonization. Infect. Immun. 76 (11), 5072–5081.
Vidovic, S., Korber, D.R., 2016. *Escherichia coli* O157: insights into the adaptive stress physiology and the influence of stressors on epidemiology and ecology of this human pathogen. Crit. Rev. Microbiol. 42 (1), 83–93.
Vong, W.C., Hua, X.Y., Liu, S.Q., 2018. Solid-state fermentation with *Rhizopus oligosporus* and *Yarrowia lipolytica* improved nutritional and flavour properties of okara. LWT-Food Sci. Technol. 90, 316–322.
Wang, C., Wang, S., Chang, T., Shi, L., Yang, H., Shao, Y., Feng, W., Cui, M., 2013. Efficacy of lactic acid in reducing foodborne pathogens in minimally processed lotus sprouts. Food Control 30 (2), 721–726.
Winder, C.L., Dunn, W.B., Schuler, S., Broadhurst, D., Jarvis, R., Stephens, G.M., Goodacre, R., 2008. Global metabolic profiling of *Escherichia coli* cultures: an evaluation of methods for quenching and extraction of intracellular metabolites. Anal. Chem. 80 (8), 2939–2948.
Zhang, J., Yang, H., 2017. Effects of potential organic compatible sanitisers on organic and conventional fresh-cut lettuce (*Lactuca sativa* Var. *Crispa* L). Food Control 72, 20–26.
Zhao, X., Wu, J.E., Chen, L., Yang, H., 2019c. Effect of vacuum impregnated fish gelatin and grape seed extract on metabolite profiles of tilapia (*Oreochromis niloticus*) fillets during storage. Food Chem. 293, 418–428.
Zhao, L., Zhang, Y., Yang, H., 2017. Efficacy of low concentration neutralised electrolysed water and ultrasound combination for inactivating *Escherichia coli* ATCC 25922, *Pichia pastoris* GS115 and *Aureobasidium pullulans* 2012 on stainless steel coupons. Food Control 73, 889–899.
Zhao, L., Zhao, M.Y., Phey, C.P., Yang, H., 2019a. Efficacy of low concentration acidic electrolysed water and levulinic acid combination on fresh organic lettuce (*Lactuca sativa* Var. *Crispa* L.) and its antimicrobial mechanism. Food Control 101, 241–250.
Zhao, L., Zhao, X., Wu, J.E., Lou, X., Yang, H., 2019b. Comparison of metabolic response between the planktonic and air-dried *Escherichia coli* to electrolysed water combined with ultrasound by ^{1}H NMR spectroscopy. Food Res. Int. 125, 108607.